PAPER

Check for updates

Synthesis and characterization of a phosphotungstic acid composite carrier and its application in solid chlorine dioxide disinfectant

Tiantian Gao,[ab] Miaomiao Hu,*[ab] Jing Tian[c] and Jintang Guo [ID] *[ab]

Chlorine dioxide (ClO_2) is an antimicrobial compound used in water. The short release time of existing solid chlorine dioxide disinfectants significantly inhibits their bactericidal efficiency. We propose a novel approach in which attapulgite was introduced into phosphotungstic acid and SBA-15 to achieve the slow-release of chlorine dioxide disinfectant tablets. The emphasis of the study lies in slow release of chlorine dioxide and reducing the escape of chlorine dioxide gas to increase the reaction time and improve disinfection efficiency. When dissolved in water the decrease rate of chlorine dioxide within 15 days after mixing SBA-15/HPW with sodium chlorite is 78.6%. Moreover, the sterilization efficiency of *Escherichia coli* reaches 100% within 5 minutes, and the killing rate of *Staphylococcus aureus* exceeds 99.999% within 10 minutes. The research solved the storage and transportation problems of ClO_2 and resulted in a solution for the disinfection of water requiring long-term disinfection.

1. Introduction

Chlorine dioxide (ClO_2) is an internationally recognized A1 grade disinfectant with high efficiency.[1,2] The high sterilization efficiency, wide range of applications,[3] and excellent safety performance make it one of the most attractive disinfectants. Since carcinogenic, teratogenic and mutagenic substances have not been detected during the sterilization process,[4–8] chlorine dioxide is an ideal disinfectant for medical treatment, food processing and preservation, water disinfection and other utilization.[9–11] However, its easy decomposition by light, strong oxidation and corrosivity make it difficult to transport and store chlorine dioxide gas at room temperature.[12] These properties inevitably increase the sterilization cost and limit its wide application.

The electron pair arrangement of ClO_2 is a planar triangle, in which Cl is sp2 hybridization,[13] and the lone electron pair occupies a hybrid orbital. The molecular shape is V-shaped, and the bond angle is 117.4°.[14] There is also a delocalized π bond in the molecule perpendicular to the molecular plane, and the bond length is 147 pm. If ClO_2 gets one electron, it will become ClO_2^-. At this time, Cl adopts sp3 hybridization, and two lone electron pairs occupy two hybrid orbitals. In ClO_2^-, the OClO bond angle is 110.5°, and the Cl–O bond length is 156 pm.[15,16] At the same time, chlorine dioxide is further stabilized, which is

also the chemical basis for preparing stable chlorine dioxide solution or solid.[5]

In solid ClO_2 tablets, ClO_2 exists temporarily in the form of ClO_2^-. The hydrolysis of ClO_2 is negligible in a relatively wide pH range from 2.0 to 10.0.[5,17] Reactive solid chlorine dioxide disinfectant was prepared by comprising reactive materials such as sodium chlorite and solid acid in a certain ratio. It was pressed into tablets or pellets and other different morphologies by adding moisture absorbent, adhesive and subsidiary materials. When placed in a humid environment, the synthesized carriers absorb moisture from the air, and ClO_2 will slowly release during the reaction. When the synthesized carriers absorbed a certain amount of water, H^+ in the support and ClO_2^- in sodium chlorite quickly diffused, and chlorine dioxide was rapidly generated in the initial stage of the reaction. The principle of reaction is shown in eqn (1).

$$5ClO^{2-} + 4H^+ = 4ClO_2 + Cl^- + 2H_2O \qquad (1)$$
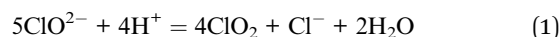
In recent years, due to their strong stability, safety and convenience, reactive solid chlorine dioxide disinfectants have attracted increasing attention. Anthony R.[18] reported that the chlorine dioxide disinfectant can be prepared by mixing lithium hypochlorite, sodium chlorite, and sodium bisulfate. Ray[19] incorporated sodium chlorite and citric acid powder into polylactic acid polymer and prepared a polylactic acid film by the solvent casting method, in which chlorine dioxide was released from the film under moisture. Bai[20] prepared a two-component system by coating sodium chlorite and tartaric acid onto an acrylate based pressure sensitive adhesive and polyvinyl alcohol. The composite of the two membranes could react to

[a] School of Chemical Engineering and Technology, Tianjin University, Tianjin 300350, China. E-mail: mmhu1990@tju.deu.cn; jtguo@tju.edu.cn

[b] Institute of Shaoxing, Tianjin University, Zhejiang 312300, China

[c] School of Biological and Environmental Engineering, Tianjin Vocational Institute, Tianjin 300410, China

generate chlorine dioxide gas in a humid environment. Huang[21] fabricated chlorine dioxide microcapsules by mixing with polylactic acid, and the release time was up to 10 days. The existing slow-release solid chlorine dioxide overcomes the shortcomings of traditional chlorine dioxide, which is not easy to store and transport. However, the corrosion of sodium chlorite and acid as raw materials in the one-pack is significant, and there are still problems to be solved, such as the need to mix raw materials, over-release phenomenon in the initial release stage and short sustained-release time. Therefore, it is very important to design a rate controllable and protracted sustained release solid chlorine dioxide disinfectant.

Heteropoly acid is a kind of acid with strong oxidation ability, high acidity and good thermal stability.[22] Under normal circumstances, heteropoly acid is loaded onto suitable carriers.[23–26] Attapulgite with large surface areas and stable chemical and mechanical properties is a kind of natural clay[27] and has extensive sources.[28] The layered hydrated magnesium aluminum silicate microstructure of attapulgite has been proved, and it consists of two bands of silica tetrahedra linked by octahedral coordination of magnesium ions.[29] Owing to the unique pore structure and one-dimensional rod-like crystal,[30,31] it can serve as an ideal adsorption material and carrier. Besides, the unique crystal structure of attapulgite makes it have a unique chemical property such as water-absorbing quality.[32]

Santa Barbara Amorphous-15 (SBA-15) is a major subset of mesoporous molecular sieves.[33] By virtue of its large specific surface areas, large pores, thick pore walls, and improved stabilities,[34] SBA-15 is often applied as an adsorbent for the separation of organics, heavy metal ions, dyes, and so on.[35–37] Due to the above advantages, SBA-15 can serve as an excellent carrier to load solid acids.

To overcome the storage and transportation problems of chlorine dioxide and achieve its wide application, the phosphotungstic acid in heteropoly acid was selected. Two kinds of carriers with excellent adsorption properties (SBA-15 and attapulgite) were combined to obtain the composite carrier. SBA-15/attapulgite/HPW was designed and synthesized, which is a chlorine dioxide disinfectant composite carrier supported by phosphotungstic acid. The textural properties and morphological structures of the composite carriers were characterized by means of scanning electron microscopy (SEM), Transmission Electron Microscopy (TEM), Brunauer–Emmett–Teller (BET) and Fourier transform infrared spectroscopy (FTIR). The effects of type of P_{123} (PEO–PPO–PEO), carrier shapes and the ratio of attapulgite on the composite carrier adsorption performance, as well as the antimicrobial effectiveness, were comprehensively investigated to determine the optimal synthesis condition. Finally, the sterilization efficiency was tested via the suspension quantitative bactericidal test.

2. Experimental

2.1 Materials

Attapulgite was purchased from Xinyuan Technology Co., Ltd, in Jiangsu Province. Tetraethyl orthosilicate (TEOS), P123, phosphotungstic acid and all of the other chemicals are all of reagent grade. All chemicals were not further purified. Distilled water and chemicals without further purification were used in this study.
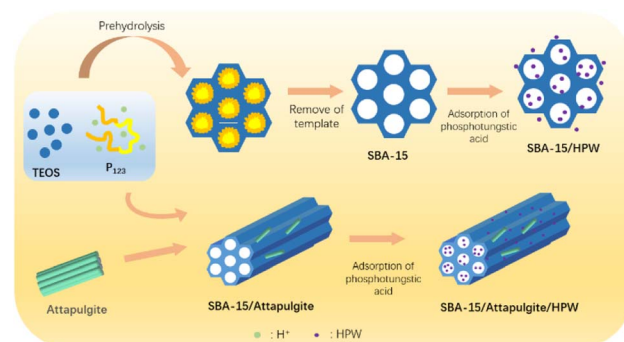
2.2 Preparation of SBA-15

The preparation process of SBA-15 has been reported by Du.[38] Tetraethyl orthosilicate (TEOS) is the silicon source and PEO–PPO–PEO copolymers (denoted as P123, $M_w = 5800$) serve as the template. Firstly, P123 was added to the HCl/water solution, and the resulting mixture was then added to the system, and magnetically stirred at a constant temperature of 35 °C for 20 hours. A large amount of white precipitate was produced at this time. The weight ratio of distilled water : concentrated hydrochloric acid : P123 : TEOS was 77.5% : 14.5% : 2.5% : 5.5%. The beaker was placed in an electrically heated blast drying oven at 100 °C to continue the reaction for 24 hours. After the sample was filtered and washed, it was calcined at 550 °C for 6 hours to obtain the final product of SBA-15.

2.3 Preparation of attapulgite/SBA-15

The preparation process of attapulgite/SBA-15 was similar to the synthesis of SBA-15 with the same weight ratio of distilled water : concentrated hydrochloric acid : P123 : TEOS. A certain amount of attapulgite was added to the system after stirring, and the reaction was continued at 100 °C for 24 hours and calcined at 550 °C for 6 hours to obtain the attapulgite/SBA-15.

2.4 Preparation of SBA-15/HPW and SBA-15/attapulgite/HPW

The wight ratio of distilled water : phosphotungstic acid : SBA-15 was 50 : 2.583 : 2. A specific amount of SBA-15 was added to the dissolved phosphotungstic acid solution, and stirred for 4 hours and then water was evaporated at 100 °C. Subsequently, drying was continued at 150 °C for 4 hours to obtain SBA-15/HPW. SBA-15/attapulgite/HPW was also obtained by a similar method. The detailed preparation process of SBA-15/HPW and SBA-15/attapulgite/HPW can be identified in a schematic illustration and is described in Scheme 1.

Scheme 1 A schematic illustration of the synthesis of SBA-15/HPW and SBA-15/attapulgite/HPW.

2.5 Quantitative measurement of ClO$_2$

In order to evaluate the stability of the chlorine dioxide disinfectant, the prepared SBA-15/HPW and SBA-15/attapulgite/HPW were uniformly mixed with a certain amount of sodium chlorite and pressed into tablets, on which the stability test was carried out. On the 1st, 2nd, 3rd, 4th, 7th, 10th, and 15th days after mixing, a fixed amount of the mixture was weighed and dissolved in a certain amount of distilled water. The concentration of chlorine dioxide in the liquid was measured with a portable chlorine dioxide colorimeter. The decrease rate of chlorine dioxide concentration was used to characterize the sustained release properties of each composite carrier.

$$\text{The decrease rate of ClO}_2 = (C_0 - C)/C_0 \times 100\% \quad (2)$$

where C_0 and C in eqn (2) are the initial concentration and final concentration of ClO$_2$.

2.6 Suspension quantitative bactericidal test

A bacterial suspension with a concentration of $\sim$108 CFU mL^{-1} was prepared. 0.5 mL of bacterial suspension and 0.5 mL of organic interfering substances were added to a sterile test tube. The solution was vortexed for 30 s to make the system evenly mixed, then 4.0 mL disinfectant was added after 5 minutes (TPS solution was used as the blank control group), and vortexed for 30 s to affect a predetermined time. 0.5 mL mixed solution was added to 4.5 mL sterilized neutralizing agent, and mixed evenly and the reaction was left for 10 minutes. Then several gradient dilutions were prepared. 1.0 mL of the mixed solution was taken to inoculate the medium, and incubated at 37 °C for 24 h.

The disinfection criterion is that the killing rate exceeds 99.999%; that is, the killing log value (KL) exceeds 5.00. The formula of killing log value is as follows:[39]

$$\text{KL} = \log M - \log N \quad (3)$$

where M and N in eqn (3) denote the average concentration of live bacteria in the control group and the average concentration of live bacteria in the test group.

3. Results and discussion

3.1 Microstructure characteristic of carriers

Fig. 1 shows the scanning electron microscopy images of SBA-15, attapulgite and SBA-15/attapulgite. As can be seen from Fig. 1a and b, the morphology and microstructure of uniform sized, spikelet shaped, short rod like SBA-15 and scattered,
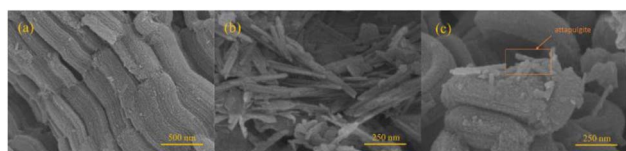

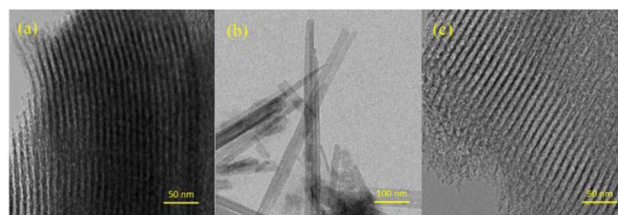**Fig. 1** SEM images of (a) SBA-15, (b) attapulgite, and (c) SBA-15/attapulgite.

Fig. 2 TEM images of (a) SBA-15, (b) attapulgite, and (c) SBA-15/attapulgite.

slender rod like attapulgite can be clearly observed. Fig. 2c is the combination of SBA-15 and attapulgite, where SBA-15 is in the form of short rods, with attapulgite surrounding it and filling the gap. The overall structure is tight, with a clear mesoporous structure. The short rod SBA-15 combines with attapulgite to form a material with stronger adsorption capacity.

Fig. 2 is the corresponding TEM of these samples. As shown in Fig. 2a, the barrier has a two-dimensional hexagonal mesoporous structure and the pore channels are arranged in a uniform order, which indicates that SBA-15 was successfully synthesized. Fig. 2b illustrates that attapulgite is a hollow tubular structure. Fig. 2c shows that the barrier also has uniform and ordered pores arranged, which indicates that the two kinds of carriers were successfully combined and did not destroy the SBA-15 crystal structure. This is consistent with the conclusion obtained by SEM images.

3.2 FT-IR of carriers

FT-IR analysis was applied to verify the microstructure of SBA-15/attapulgite/HPW in the reaction process. As shown in Fig. 3, the peak of the vibration of P–O can be found at 1080 cm^{-1}, and the absorption peak at 985 cm^{-1} is caused by W=O vibration. Peaks at 899 cm^{-1} and 805 cm^{-1} can be assigned to the asymmetric stretching vibration of W–O–W, respectively. The above four characteristic peaks are attributed to the asymmetric vibration absorption of phosphotungstic acid Keggin structure.
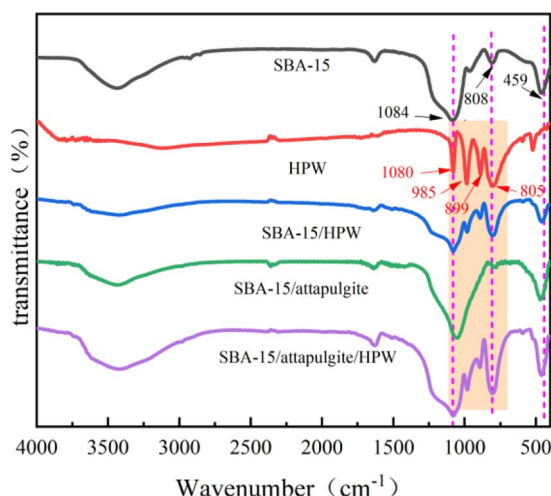

Fig. 3 FT-IR characterization of phosphotungstic acid series carriers.

Comparing the FT-IR spectra of SBA-15 with SBA-15/HPW, the latter has two new absorption peaks at 983 cm^{-1} and 892 cm^{-1}, which correspond exactly to the characteristic peaks of the pure phosphotungstic acid Keggin structure. The absorption peaks of SBA-15/HPW at 1080 cm^{-1} and 803 cm^{-1} are broader and their intensity is also higher than that of SBA-15. This is because the Si–O–Si in SBA-15 has antisymmetric stretching vibration and symmetric stretching vibration at 1084 cm^{-1} and 808 cm^{-1}, respectively, which are caused by the superposition of P–O and W–O–W of phosphotungstic acid. In addition, SBA-15/HPW shows a strong absorption peak at 459 cm^{-1}, which is attributed to the bending vibration of Si–O. This result indicates that the synthesized SBA-15/HPW sample retains the mesoporous framework structure of SBA-15 and also shows the presence of phosphotungstic acid.

Observing the FT-IR of SBA-15/attapulgite and SBA-15/attapulgite/HPW, it is found that the latter has three new characteristic absorption peaks at 982 cm^{-1}, 894 cm^{-1} and 804 cm^{-1}. These correspond to the characteristic absorption peaks of the pure phosphotungstic acid Keggin structure at 985 cm^{-1}, 889 cm^{-1} and 805 cm^{-1}, respectively. The absorption peak of SBA-15/attapulgite/HPW at 1080 cm^{-1} is wider than the peak of SBA-15/attapulgite at this position, which is caused by the superposition of Si–O–Si and P–O of phosphotungstic acid. In addition, a strong absorption peak formed by the bending vibration of Si–O appeared at 461 cm^{-1}, which proves that the SBA-15/attapulgite/HPW samples retain both the characteristic skeleton structure of SBA-15/attapulgite and the Keggin structure of phosphotungstic acid.

3.3 BET of SBA-15/HPW and SBA-15/attapulgite/HPW

The Brunauer–Emmett–Teller (BET) gas adsorption method was used to measure the porous characteristics of two loaded solid acid samples (SBA-15/attapulgite and SBA-15/attapulgite/HPW). Fig. 4 reports the N_2 adsorption–desorption isotherms. The N_2 adsorption–desorption isotherms are classified as type IV.[40] The specific feature in Fig. 4 is the hysteresis loop, which is the typical feature of mesoporous materials. When the relative pressure is close to 1, the curve rises dramatically, indicating that there are macropores and probably the macropores are ascribed to the gaps between particles.

Based on the above analysis, the prepared phosphotungstic acid composite carrier is a mesoporous material, and the distribution of mesopores is relatively uniform.
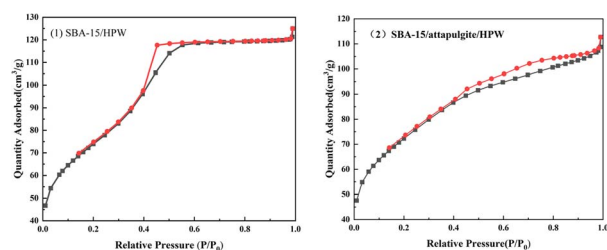
The pore diameter distributions of the samples are shown in Fig. 5. Based on the IUPAC nomenclature, mesoporous material nanostructures with pore diameters ranging from 2 to 50 nm can be defined by mesoporous materials.[41] The results show that the pore diameters of the two samples are gathered in the range of 3–4.5 nm, which proves that the two synthesized phosphotungstic acid composite supports are typical mesoporous materials. The mesoporous uniformity was further demonstrated, and the result was consistent with the nitrogen adsorption and desorption curves.

The results of the specific surface area analysis are shown in Table 1. It can be seen from Table 1 that the average pore diameter of the phosphotungstic acid composite carriers is in the range of 3–4 nm, which further shows that the synthesized sample is mesoporous.

The relevant parameters of SBA-15 and SBA-15/attapulgite were also compared in this part. The sample with SBA-15/attapulgite as a carrier has larger pore volume and pore diameter than the sample with SBA-15 as the carrier, regardless of being loaded with phosphotungstic acid or not. The larger specific surface area and larger pore volume make it possible to load more phosphotungstic acid, which in turn produces more chlorine dioxide disinfectant in subsequent reactions. Therefore, the composite carrier obtained by combining SBA-15 and the attapulgite has better adsorption performance.

The pore volume and pore diameter of the samples loaded with phosphotungstic acid on SBA-15 and SBA-15/attapulgite
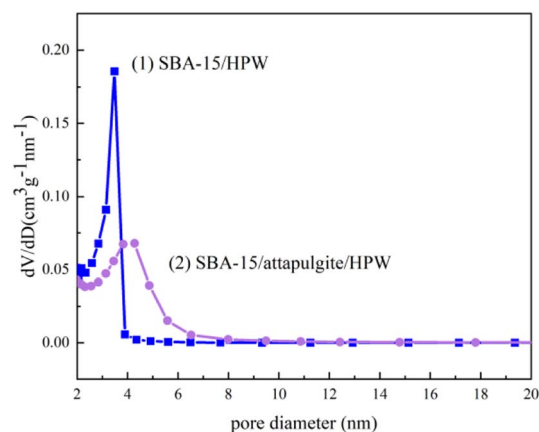

Fig. 5 Pore diameter distribution of the two loaded phosphotungstic acid samples.

Fig. 4 N_2 adsorption and desorption isotherms of loaded phosphotungstic acid samples.

Table 1 Results of specific surface area

Samples	Specific surface area (m^2 g^{-1})	Pore vol (cm^3 g^{-1})	Pore diameter (nm)
SBA-15	753.34	0.706	3.85
SBA-15/attapulgite	658.19	0.732	4.29
SBA-15/HPW	262.99	0.163	3.18
SBA-15/attapulgite/HPW	252.95	0.188	3.74

decrease when compared to the samples before loading. This indicates that phosphotungstic acid has entered the internal pore of the carrier, rather than simply adsorbed on the surface of the carrier.

3.4 Factors affecting the performance of SBA-15/attapulgite/HPW

3.4.1 Effect of the type of P123 and carrier shapes. During the synthesis of SBA-15, P123 (PEO–PPO–PEO) as a template agent plays a decisive role in the pore formation of mesoporous materials. After P123 is dissolved in water, micelles will be formed due to the spatial effect, intermolecular interaction and entropy interaction. The hydrophilic PEO units form a corona, while hydrophobic PPO units form cores in the micelle. During the mesostructure formation, the units serve as the silica deposition sites.[42] Tetraethyl orthosilicate was polycondensated and solidified near the hydrophilic chain to obtain the pore wall structure of mesoporous materials. Finally, the template was removed at 550 °C roasting temperature in a muffle furnace to obtain mesoporous SBA-15.

Commercially available P_{123} (M_w = 5800 or 9800) was used to synthesize particulate and powdered supports by mechanical or magnetic stirring. The influence of the template agent and the shape of the composite carrier on the carrier performance was explored by BET tests and chlorine dioxide concentration tests.

Table 2 shows that except the pore volume of particle 9800 is a little smaller than that of particle 5800, the values of specific

Table 2 Summary of BET result parameters of samples with different templates and carrier shapes

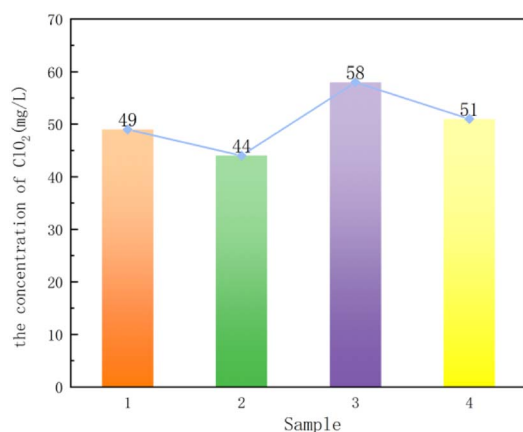| Samples	Specific surface area ($m^2 g^{-1}$)	Pore vol ($cm^3 g^{-1}$)	Pore diameter (nm)
Powder 5800	93	0.0577	3.87
Powder 9800	75	0.0522	3.68
Particle 5800	118	0.0667	4.40
Particle 9800	127	0.0600	4.94

Fig. 6 Effects of template and carrier shapes on the concentration of ClO_2 in tablets (1: powder 5800; 2: powder 9800; 3: particle 5800; 4: particle 9800).

surface area and pore diameter are the largest, indicating that the adsorption effect is the best.

Fig. 6 shows that the chlorine dioxide concentration of sample 1 is higher than that of sample 2, and the chlorine dioxide concentration of sample 3 is higher than that of sample 4, which corresponds to the results of BET. In addition, the results of BET and chlorine dioxide concentration show that sample 3 and sample 4 are better than sample 1 and sample 2, indicating that the particle composite carrier is better when loading solid acid. In conclusion, the granular composite carrier synthesized with P_{123} (M_w = 5800) as the template has better adsorption performance.

3.4.2 Effect of the ratio of attapulgite. Due to large surface areas and pores inside,[28] attapulgite can adsorb a lot of substances. In order to combine the properties of attapulgite and SBA-15, attapulgite was added to the solution to obtain a composite carrier. The effects of different amounts of attapulgite on the structure of the composite carrier and the properties of supported phosphotungstic acid were investigated. The proportions of attapulgite and TEOS in samples 1–5 are 1: 25, 2: 25, 3: 25, 4: 25 and 5: 25 respectively.

Table 3 shows that with more addition of attapulgite, the specific surface area shows a tendency to rise first, then decrease and then rise. Considering the reason that the specific surface area of attapulgite is larger, the more the addition of it, the larger the specific surface area of the composite. But when the addition amount exceeded a certain value, too much attapulgite affected the formation of SBA-15, so the specific surface area of the composite support decreased. When the addition amount of attapulgite continued to increase, the influence of the formation of SBA-15 on the overall specific surface area weakened, so the specific surface area of the composite support again showed an increasing trend with the addition amount. While the amount of attapulgite continues to increase, the effect of the formation of SBA-15 on the overall specific surface area becomes weak, and the specific surface area mainly due to the increase of the amount of attapulgite. The trends of pore volume and specific surface area are similar. The microstructure of sample 2 is more favorable for loading and adsorption than the others with the BET test.

The five composite supports were loaded with phosphotungstic acid and pressed by mixing with sodium chlorite, and tablets were dissolved in water to measure the concentration of ClO_2. Fig. 7 shows that the concentration of ClO_2 is 2 > 5 > 3 > 4 > 1, where only the order of sample 1 and sample 4 was changed

Table 3 Summary of BET result parameters of samples with different templates and carriers

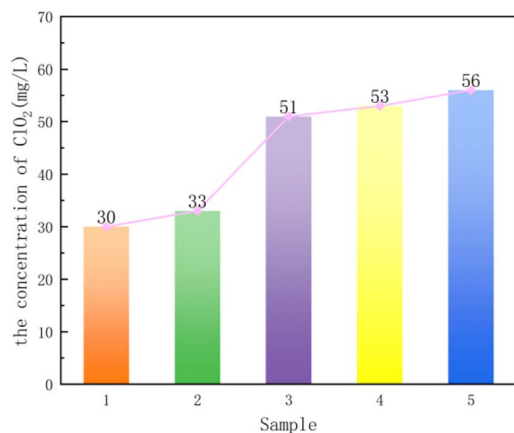| Samples	Specific surface area ($m^2 g^{-1}$)	Pore vol ($cm^3 g^{-1}$)	Pore diameter (nm)
1	152	0.0674	3.45
2	204	0.1033	3.54
3	127	0.0600	4.94
4	103	0.0710	5.55
5	192	0.0808	4.09

Fig. 7 Effect of attapulgite addition on the concentration of ClO$_2$ in tablets (the proportions of attapulgite and TEOS in samples 1–5 are 1: 25, 2: 25, 3: 25, 4: 25 and 5: 25, respectively).

according to the result of the specific surface area. The reason is that when the specific surface areas differs less, the supports with large pore volume and large pore size are more favorable for the entry of phosphotungstic acid molecules. Finally, from the results of BET and the concentration of ClO$_2$, the best performance of the composite support was obtained when the attapulgite to TEOS ratio was 2 : 25.

3.5 Quantitative measurement of ClO$_2$ released from powdered precursors

The mass ratio of HPW to NaClO$_2$ is about 3 : 1 according to the production formula that the maximum molar ratio of HPW is 3.5.[43] Solid ClO$_2$ tablets were prepared according to the calculated formula and put into a certain amount of water. Fig. 8 shows the slow release of chlorine dioxide after SBA-15/ attapulgite/HPW and SBA-15/HPW are mixed with sodium chlorite and dissolved in water. As shown in Fig. 8, the decrease rate of chlorine dioxide within 15 days after mixing SBA-15/ HPW with sodium chlorite is 78.6%. In contrast, the decrease
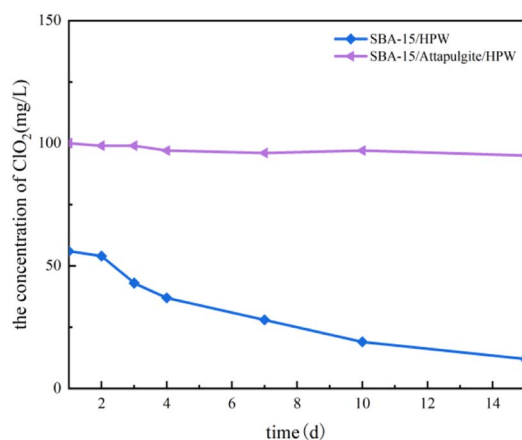

Fig. 8 Chlorine dioxide release diagram of the phosphotungstic acid composite carrier.

rate of ClO$_2$ is only 5% within 15 days when SBA-15/attapulgite/ HPW is used as the carrier. This shows that the sample with SBA-15/attapulgite/HPW as the carrier produced more ClO$_2$ and has a lower decrease rate than the sample with SBA-15/HPW as the carrier. This proves that the addition of attapulgite has a decisive effect on the slow-release performance of the sample in producing chlorine dioxide. In other words, the stability of the sample obtained with SBA-15/attapulgite/HPW as the carrier is higher than that of the one prepared using SBA-15/HPW.

3.6 Antimicrobial effectiveness of the chlorine dioxide disinfectant

The bactericidal performance of the chlorine dioxide disinfectant was studied. Sodium chlorite and SBA-15/attapulgite/HPW were mixed and compressed to prepare solid chlorine dioxide disinfectant tablets. The chlorine dioxide solution prepared by dissolving in water was used as a disinfectant. Furthermore, phosphotungstic acid was replaced by citric acid and oxalic acid with equal H$^+$ numbers as control groups.

Three kinds of disinfection solutions were tested for the suspension quantitative bactericidal test.

Escherichia coli and *Staphylococcus aureus* were used as experimental strains. They represent Gram-negative bacteria and Gram-positive bacteria respectively. In order to eliminate the error caused by the residual disinfectant in the experimental results, it is necessary to immediately add a qualified neutralizer at the end of the designated sterilization. Through the preliminary selection experiment of the neutralizer and the neutralizer identification experiment,[39] PBS solution containing 0.5% of Na$_2$S$_2$O$_3$, 0.2% of lecithin, and 2% of Tween-80 was selected.

The results are shown in Fig. 9A (*Escherichia coli*) and Fig. 9B (*Staphylococcus aureus*). As shown in Fig. 9, sample 1 uses the phosphotungstic acid composite carrier as the acid source, sample 2 uses citric acid as the acid source, and sample 3 uses oxalic acid as the acid source.

The effects of the three solutions after mixing with the *Escherichia coli* suspension for 5 minutes are shown in Fig. 9A. As shown in Fig. 9A, the *E. coli* killing rate of sample 1 reaches 100%. However, the bactericidal effects of sample 2 and sample 3 are not obvious, and the average killing log values are both lower than 5.00. The sterilization results of *Staphylococcus aureus* are shown in Fig. 9B. After the three solutions were mixed with the bacterial suspension for 10 minutes, the average log killing value of sample 1 was higher than 5.00. This means that sample 1 is qualified for sterilization. However, sample 2 and sample 3 do not achieve the disinfection effect. The reason is that the acidity of the phosphotungstic acid is much stronger than that of oxalic acid and citric acid. It has been shown that the more the acidity the more the H$^+$ provided, the better the activation of ClO$_2$$^-$ and the more the ClO$_2$ released. The activation is complete within 5 min at pH < 0.5, and the reaction is not complete after 1 h at pH > 1.[44] ClO$_2$ can kill *Escherichia coli* and *Staphylococcus aureus* in a wide range of pH from 3 to 9.[45] And the decomposition rate of ClO$_2$ is a function of pH and temperature. When the temperature is certain, the lower the
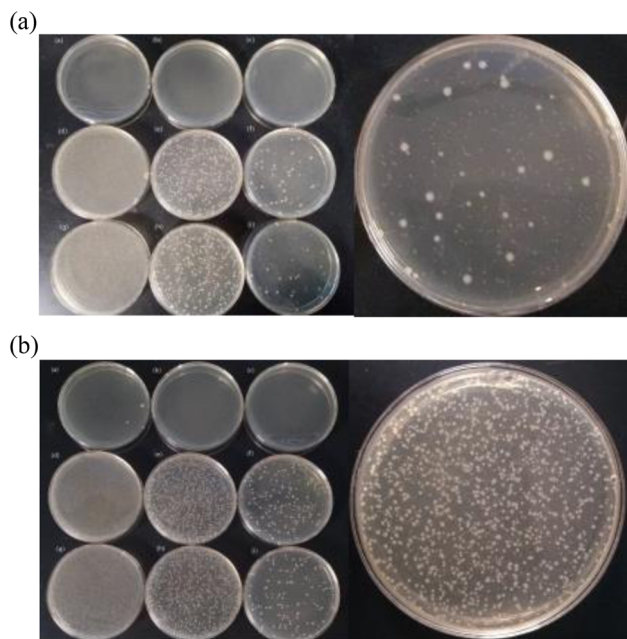
Paper

(a)

(b)

Fig. 9 (A) Suspension quantitative sterilization test of *Escherichia coli* (a)–(i) sample 1-10^{-1}, 1-10^{-2}, 1-10^{-3}, 2-10^{-1}, 2-10^{-2}, 2-10^{-3}, 3-10^{-1}, 3-10^{-2}, and 3-10^{-3}, and the right figure is blank control group-10^{-4}. (B) Suspension quantitative sterilization test of *Staphylococcus aureus* (a)–(i) sample 1-10^{-1}, 1-10^{-2}, 1-10^{-3}, 2-10^{-1}, 2-10^{-2}, 2-10^{-3}, 3-10^{-1}, 3-10^{-2}, and 3-10^{-3}, and the right figure is blank control group-10^{-4}.

pH, the more the chlorine dioxide released. Thus, HPW ionizes more H^+ and its activation is better under the same conditions. When there is the same amount of acid source, the acidity of citric acid and oxalic acid is not strong enough to activate sodium chlorite to produce an equal amount of chlorine dioxide. Therefore, the sterilization of the solution is low. On the contrary, the solution prepared by using the phospho-tungstic acid composite carrier as the acid source achieves a better sterilization effect. The concentration of chlorine dioxide is determined as follows. The concentration of sample 1 is 31 mg L^{-1}, and the concentrations of sample 2 and sample 3 are close to zero, which also verifies the above statement.

4. Conclusions

In this paper, SBA-15 and attapulgite were combined to construct a composite carrier SBA-15/attapulgite with better comprehensive performance, which was used to load phosphotungstic acid and achieve slow-release of ClO$_2$. The conclusions can be drawn as follows.

(1) The phosphotungstic acid has been loaded on the corresponding carriers *via* solution adsorption. Both synthesized carriers are mesoporous materials with pore diameters between 3 and 4 nm.

(2) The solid acid is not only loaded on the surface of the carrier, but also enters the internal pore structure. The addition of attapulgite has a decisive effect on the slow-release performance of the sample. In addition, the solid obtained by mixing

SBA-15/attapulgite/HPW with sodium chlorite has a higher concentration of ClO$_2$, which can be kept stable for a long time.

(3) The killing rate of *Escherichia coli* in 5 minutes reaches 100%, and the killing rate of *Staphylococcus aureus* in 10 minutes exceeds 99.999%. The bactericidal effect is better than that of the chlorine dioxide disinfectant prepared by citric acid and oxalate acid with the same H^+ concentration.

By way of closure to this study, the work presents a systematic investigation into the application of SBA-15/attapulgite to achieve the slow release of ClO$_2$. This might provide a novel approach to exploring more molecular sieves for disinfection for various water treatment and air sterilization. Moreover, it could provide a theoretical basis and reference for further improvement of industrial implementation and controlling the release rate of chlorine dioxide.

Author contributions

Tiantian Gao-data curation, formal analysis, investigation, methodology, and writing-original draft. Miaomiao Hu-formal analysis, conceptualization, and writing-review & editing. Jing Tian -investigation. Jintang Guo-project administration, writing—review & editing, supervision, and conceptualization.

Conflicts of interest

There are no conflicts to declare.

Acknowledgements

References

1 S. D. Richardson, A. D. Thruston and T. W. Collette, *Environ. Sci. Technol.*, 1994, **28**, 592–599.
2 J. Huang, W. Li, N. Ren, L. X. Li and G. Yang, *Water Res.*, 1997, **31**, 455–460.
3 M. E. B. Parish, T. V. Suslow, L. J. Harris, E. H. Garrett, J. N. Farber and F. F. Busta, *Compr. Rev. Food Sci. Food Saf.*, 2003, **2**, 161–173.
4 T. Ozawa, Y. Miura and J. I. Ueda, *Free Radical Biol. Med.*, 1996, **20**, 837–841.
5 W. Gan, Y. Ge, Y. Zhong and X. Yang, *Environ. Sci.: Water Res. Technol.*, 2020, **6**, 2287–2312.
6 X. Sun, E. Baldwin, C. Ference, J. Narciso, A. Plotto, M. Ritenour, K. Harrison, D. Gangemi and J. Bai, *HortScience*, 2017, **52**, 122–126.
7 M. Benarde, *Appl. Microbiol.*, 1967, **15**, 257–265.
8 K. V. Sy, K. H. Mcwatters and L. R. Beuchat, *J. Food Prot.*, 2005, **68**, 1165–1175.
9 L. S. Tsai, R. Higby and J. Schade, *J. Agric. Food Chem.*, 1995, **43**, 2768–2773.
10 L.-S. Tsai, B. Hernlem and C. C. Huxsoll, *J. Food Sci.*, 2002, **67**, 2160–2164.

11 J. Kim, M. R. Marshall, W. X. Du, W. S. Otwell and C. I. Wei, *J. Agric. Food Chem.*, 1999, **47**, 3586–3591.

12 A. Tomás-Callejas, F. López-Gálvez, A. Sbodio, F. Artés, F. Artés-Hernández and T. V. Suslow, *Food Control*, 2012, **23**, 325–332.

13 V. Vaida and J. D. Simon, *Science*, 1995, **268**, 1443–1448.

14 M.-Y. Xu, Y.-L. Lin, T.-Y. Zhang, C.-Y. Hu, Y.-L. Tang, J. Deng and B. Xu, *J. Hazard. Mater.*, 2022, **436**, 129195.

15 G. Ziyi, *J. Inn. Mong. Norm. Univ.*, 1989, **1**, 55–59.

16 G. Ziyi, *Chem. Bull.*, 1984, **05**, 126–127.

17 J. Schijven, P. Teunis, T. Suylen, H. Ketelaars, L. Hornstra and S. Rutjes, *Water Res.*, 2019, **158**, 34–45.

18 A. R. Pitochelli, *US Pat.*, US6602442, 2003.

19 J. T. Ray, S. X. Fan, *et al.*, *J. Food Sci.*, 2013, **78**, 276–284.

20 Z. Bai, D. E. Cristancho, A. A. Rachford, A. L. Reder, A. Williamson and A. L. Grzesiak, *J. Agric. Food Chem.*, 2016, **64**, 8647–8652.

21 C. Huang, B. Zhang, S. Wang, L. Zhang, J. Wang, X. Huang, Y. Zhao and L. Huang, *J. Mater. Sci.*, 2018, **53**, 12704–12717.

22 S. Silva, A. Chaumonnot, A. Bonduelle-Skrzypczak, F. Lefebvre, S. Loridant and V. Dufaud, *ChemCatChem*, 2014, **6**, 464–467.

23 J. Ding, T. Ma, S. Rong, X. Wei, P. Wang, X. Song, R. Guan, K. Yeung and H. Wei, *New J. Chem.*, 2018, **42**, 14271–14280.

24 L. Cheng and R. Wang, *Int. J. Nanosci.*, 2012, **11**, 1240030.

25 A. C. Garade, V. S. Kshirsagar, A. Jha and C. V. Rode, *Catal. Commun.*, 2010, **11**, 942–945.

26 B. Li, Z. Liu, C. Han, J. Liu, S. Zuo, Z. Zhou and X. Pang, *J. Mol. Catal. A: Chem.*, 2011, **348**, 106–113.

27 R. K. Gogoi and K. Raidongia, *Adv. Mater.*, 2017, **29**, 1701164.

28 W. Wang, H. Chen and A. Wang, *Sep. Purif. Technol.*, 2007, **55**, 157–164.

29 Y. Zhu, T. Chen, H. Liu, B. Xu and J. Xie, *J. Mol. Liq.*, 2016, **219**, 272–278.

30 X. Wu, W. Zhu, X. Zhang, T. Chen and R. L. Frost, *Appl. Clay Sci.*, 2011, **52**, 400–406.

31 J. Dong, Q. Zhu, Q. Wei, B. Zheng, S. Li and J. Zhang, *Appl. Clay Sci.*, 2018, **165**, 8–16.

32 S. Q. Gu, X. N. Kang, L. Wang, E. Lichtfouse and C. Y. Wang, *Environ. Chem. Lett.*, 2019, **17**, 629–654.

33 N. Rahmat, A. Z. Abdullah and A. R. Mohamed, *Am. J. Appl. Sci.*, 2010, **7**, 1579–1586.

34 M. B. Nguyen, P. Xuan Nui and H. V. Doan, *RSC Adv.*, 2021, **11**, 31738–31745.

35 M. Li, P. J. Pham, C. U. Pittman Jr and T. Li, *Microporous Mesoporous Mater.*, 2009, **117**, 436–443.

36 S. Masoudnia, M. H. Juybari, R. Z. Mehrabian, M. Ebadi and F. Kaveh, *Int. J. Biol. Macromol.*, 2020, **165**, 118–130.

37 A. Tanimu and K. Alhooshani, *Microchem. J.*, 2020, **159**, 105410.

38 G. Du, S. Lim, M. Pinault, C. Wang, F. Fang, L. Pfefferle and G. L. Haller, *J. Catal.*, 2008, **253**, 74–90.

39 G. D., *Standardization for Sterilization Technique*, 2012, pp. 26–34.

40 J. Meng, F. Fang, N. Feng, H. Wan and G. Guan, *RSC Adv.*, 2020, **10**, 2472–2482.

41 Z. Wu and D. Zhao, *Chem. Commun.*, 2011, **47**, 3332–3338.

42 Y. Wan and D. Zhao, *Chem. Rev.*, 2007, **107**, 2821–2860.

43 P. L. Wang and J. F. Sichuan, *Chem*, 2021, **24**, 50–55.

44 G. Gordon, R. G. Kieffer and D. H. Rosenblatt, *The chemistry of chlorine dioxide*, John Wiley & Sons, 1972, pp. 141–142.

45 W. L. Huang Junli, *China Water Supply and Drainage*, 1996, **12**, 4–7.